Improvements and limitations of Mie n-6 force fields for predicting liquid shear viscosity at saturation and elevated pressures

Richard A. Messerly

Thermodynamics Research Center, National Institute of Standards and Technology, Boulder, Colorado, 80305

Michelle C. Anderson

Thermodynamics Research Center, National Institute of Standards and Technology, Boulder, Colorado, 80305

S. Mostafa Razavi

Department of Chemical and Biomolecular Engineering, The University of Akron

J. Richard Elliott

Department of Chemical and Biomolecular Engineering, The University of Akron

Abstract

While many common force fields are developed based only liquid density and heat of vaporization at room temperature, several more recent force fields have taken into account saturated vapor pressure and saturated liquid density over substantial portions of the vapor-liquid coexistence curve for multiple compounds simultaneously, enhancing transferability. This manuscript explores the hypothesis that greater accuracy in characterizing the coexistence properties may lead to greater accuracy for viscosity predictions. Three united atom force fields are considered in detail: the TraPPE-UA model of Siepmann and coworkers, the TAMie model of Gross and coworkers, the AUA4 model of Ungerer and coworkers, and the TraMie model of Potoff and coworkers. Equilibrium molecular dynamics simulations are performed in the NVT ensemble using the Green-Kubo method for viscosity characterization. Simulations are performed for linear alkanes with two to sixteen carbons and branched

Email addresses: richard.messerly@nist.gov (Richard A. Messerly), michelle.anderson@nist.gov (Michelle C. Anderson), sr87@uakron.edu (S. Mostafa Razavi), elliot1@uakron.edu (J. Richard Elliott)

alkanes with four to nine carbons. Simulation conditions follow the saturated liquid from reduced temperatures of 0.5 to 0.9 and along the 293 K isotherm in the dense liquid region.

In general, the more accurate force fields for coexistence properties do indeed predict viscosity more accurately. For saturated liquids, both the TraMie and TAMie models provide roughly 10 % accuracy for linear alkanes, while deviations are closer to 20 to 50 % for AUA4 and TraPPE-UA models. For branched alkanes, the behavior is more complicated but TraMie still provides roughly 15 to 20 % accuracy, while the TAMie force field results in deviations of 20 to 40 %, and the TraPPE-UA and AUA4 force fields have deviations of approximately 25 to 60 %. The deviations tend to increase with decreasing temperature, with the exception of the TraMie deviations for propane, which are nearly constant to the triple point temperature.

For compressed liquids, the Mie potential models perform better once again, but tend to overestimate the viscosity at very high densities. Coincidentally, these models also tend to overestimate the pressure at high densities, such that plots of viscosity with respect to pressure are accurate to within about 10 % up to 200 MPa. Experimental viscosity data tend to be sparse above 200 MPa, but accurate predictions are obtained for propane to 1 GPa. Uncertainty estimates increase substantially for high pressures at low reduced temperatures. Nevertheless, a prediction is made for the viscosity of 2,2,4-trimethylpentane at 293K and 1 GPa.

Keywords:

Thermophysical Properties, Molecular Simulation

---

1. Introduction

The design of efficient and reliable technical processes requires accurate estimates of thermophysical properties. Shear viscosity (η) is an important property for characterizing flow, e.g. sizing pumps. There are primarily three different means by which shear viscosity estimates are obtained: experimental measurement, semi-empirical model prediction, and molecular simulation (molecular dynamics, MD). Significant limitations exist for each of these methods. For example, experimental measurements can be expensive, time-consuming, and challenging at extreme temperatures (T) and pressures (P). Semi-empirical models often

struggle from poor extrapolation due to model deficiencies, over-fitting, and the scarcity of *reliable* experimental data over a wide range of $P\rho T$ state space. Molecular dynamics requires extremely reliable force fields and robust simulation methods.

There are two fundamental challenges for utilizing molecular simulation to estimate viscosity. First, obtaining reproducible results is more difficult for transport properties, such as viscosity, than for static properties. Second, viscosity is extremely sensitive to the force field. In addition to the strong dependence on the intermolecular interactions, the intramolecular potential plays a much greater role for viscosity than for static properties. For example, varying the torsional potential has a significant impact on viscosity while vapor-liquid coexistence is relatively unaffected. Therefore, the ability to predict viscosities with molecular simulation requires both robust methods and adequate force fields.

Recently, a "Best Practices Guide" was developed to address the first challenge, namely, to improve reproducibility [1]. While we apply the "Best Practices", the focus of this study is the second challenge. Specifically, we investigate the accuracy of united-atom Mie n-6 force fields, a popular class designed for the engineering purpose of predicting thermophysical properties. The suitability of these force fields for quantitative viscosity prediction has been widely debated in the literature. For example, BLANK suggested that united-atom models are inadequate for this purpose and recommended the use of all-atom models. By contrast, Reference 2 suggested that great improvement is obtained by utilizing a Mie n-6 potential over the traditional Lennard-Jones 12-6 potential. However, these studies focused on viscosities of saturated liquids. Recently, it was shown that Mie n-6 potentials are overly repulsive at high densities/pressures. For these reasons, we study how well the united-atom Mie n-6 potentials perform both at saturation and elevated pressures.

Some studies have suggested that united-atom models are not capable of accurately reproducing viscosity and, therefore, anisotropic-united-atom or all-atom models are needed [3, 4, 5]. However, other studies have shown that with the appropriate tuning of the united-atom Mie n-6 parameters viscosity can be accurately predicted without significant deprecation of other properties [2]. [6] discusses different test cases (i.e. state points, compound

structures) where united-atom or anisotropic-united-atom models are adequate and inadequate for predicting viscosity.

Furthermore, Reference 7 demonstrated that it is important to include viscosity data when parameterizing a Mie n-6 force field to obtain a unique set of transferable parameters. The force fields compared in this study were optimized solely with static vapor-liquid coexistence data, e.g., saturated liquid densities and saturated vapor pressures. Therefore, an additional purpose of this study is to determine the transferability of these force fields that were not parameterized without viscosity data.

While the Potoff and TAMie force fields have shown considerable promise in predicting vapor-liquid equilibria and other static properties, their ability to predict dynamic properties, such as viscosity, has not been investigated previously.

Previously, AUA4 developed a modified torsional potential to improve prediction of viscosity. One purpose of this study is to determine if the state-of-the-art Mie potentials are adequate of predicting viscosity without modifying the torsional potential.

The outline for the present work is the following. Section 2 explains the force fields, simulation methodology, and data analysis. Section 3 presents the simulation results for each force field, compound, and state point studied. Section 4 discusses some important observations and limitations. Section 5 recaps the primary conclusions from this work.

2. Methods

2.1. Force field

A united-atom (UA) or anisotropic-united-atom (AUA) representation is used for each compound studied. UA models assume that the UA interaction site is that of the carbon atom, while AUA models assume that the AUA interaction site is shifted away from the carbon atom and towards the hydrogen atom(s). Note that TraPPE and Potoff are UA force fields while TraPPE-2, AUA4, and TAMie are AUA force fields.

The UA and AUA groups required for normal and branched alkanes are sp^3 hybridized CH_3, CH_2, CH, and C sites. For most literature models, a single (transferable) parameter set

is assigned for each interaction site. However, two exceptions exist for the force fields studied. First, TAMie implements a different set of CH_3 parameters for ethane. Second, Potoff reports a "generalized" and "short/long" (S/L) CH and C parameter set. The Potoff "generalized" CH and C parameter set is an attempt at a completely transferable set. However, since the "generalized" parameters performed poorly for some compounds, the S/L parameter set was proposed, where the "short" and "long" parameters are implemented when the number of carbons in the backbone is ≤ 4 and > 4, respectively.

A fixed bond-length is used for each bond between UA or AUA sites. Note that, although static thermodynamic properties are generally insensitive to the choice of fixed or flexible bonds, dynamic properties, such as viscosity, are much more sensitive. For this reason, we test the degree of variability that arises by implementing a harmonic oscillator model. The results are provided as Supporting Information.

Although TAMie is an AUA force field, only the terminal CH_3 sites have a displacement in the interaction site. This convention is much simpler to implement than other AUA approaches (such as AUA4) where non-terminal (i.e. CH_2 and CH) interaction sites also have a displacement distance. For this reason, we do not attempt to simulate the AUA4 force field for any compounds containing CH_2 and CH interaction sites. For the compounds and force fields simulated, the anisotropic shift in a terminal interaction site (i.e. CH_3) is treated simply as a longer effective bond-length (see Table 1). The bond-length for all non-terminal sites is 0.154 nm.

The angle and dihedral energies are computed using the same functional forms for each force field. Angular bending interactions are evaluated using a harmonic potential:

$$u^{\text{bend}} = \frac{k_\theta}{2}\left(\theta - \theta_0\right)^2 \tag{1}$$

where u^{bend} is the bending energy, θ is the instantaneous bond angle, θ_0 is the equilibrium bond angle, and k_θ is the harmonic force constant which is equal to 62500 K/rad^2 for all bonding angles. Dihedral torsional interactions are determined using a cosine series:

$$u^{\text{tors}} = c_0 + c_1[1 + \cos\phi] + c_2[1 - \cos 2\phi] + c_3[1 + \cos 3\phi] \tag{2}$$

Table 1: Effective bond-lengths in units of nm for terminal (CH_3) UA or AUA interaction sites. Empty table entries for TraPPE-2 denote that the force field does not contain the corresponding interaction site type. Empty table entries in AUA4 arise because this force field uses a more complicated construction than the simple effective bond-length approach. Specifically, AUA4 requires CH_2 and CH interaction sites that are not along the C-C bond axis.

Bond	TraPPE, Potoff	TAMie	AUA4	TraPPE-2
CH_3-CH_3	0.154	0.194	0.1967	0.230
CH_3-CH_2	0.154	0.174	–	–
CH_3-CH	0.154	0.174	–	–
CH_3-C	0.154	0.174	0.1751	–

where u^{tors} is the torsional energy, ϕ is the dihedral angle and c_i are the Fourier constants. The equilibrium bond angles and torsional parameters are found in Tables 2-3, respectively.

Table 2: Equilibrium bond angles (θ_0). x and y are values between 0-3.

Bending sites	θ_0 (degrees)
CH_x-CH_2-CH_y	114.0
CH_x-CH-CH_y	112.0
CH_x-C-CH_y	109.5

Non-bonded interaction energies and forces between sites located in two different molecules or separated by more than three bonds are calculated using a Mie n-6 potential (of which the Lennard-Jones, LJ, 12-6 is a subclass) [8]:

$$u^{\text{vdw}}(\epsilon, \sigma, n; r) = \left(\frac{\text{n}}{\text{n}-6}\right)\left(\frac{n}{6}\right)^{\frac{6}{n-6}} \epsilon \left[\left(\frac{\sigma}{r}\right)^{\text{n}} - \left(\frac{\sigma}{r}\right)^{6}\right] \tag{3}$$

where u^{vdw} is the van der Waals interaction, σ is the distance (r) where $u^{\text{vdw}} = 0$, $-\epsilon$ is the energy of the potential at the minimum $\left(\text{i.e. } u^{\text{vdw}} = -\epsilon \text{ and } \frac{\partial u^{\text{vdw}}}{\partial r} = 0 \text{ for } r = r_{\text{min}}\right)$, and

Table 3: Fourier constants (c_i) in units of K. x and y are values between 0-3.

Torsion sites	c_0	c_1	c_2	c_3
CH_x-CH_2-CH_2-CH_y	0.0	355.03	-68.19	791.32
CH_x-CH_2-CH-CH_y	-251.06	428.73	-111.85	441.27
CH_x-CH_2-C-CH_y	0.0	0.0	0.0	461.29
CH_x-CH-CH-CH_y	-251.06	428.73	-111.85	441.27

n is the repulsive exponent. The non-bonded Mie n-6 force field parameters for TraPPE, TraPPE-2, Potoff, AUA4, and TAMie are provided in Table 4.

Table 4: Non-bonded (intermolecular) parameters for TraPPE [9, 10] (and TraPPE-2 [11]), Potoff [12, 13], AUA4 [14, 15], and TAMie [16, 17] force fields. The "short/long" Potoff CH and C parameters are included in parentheses. The ethane specific parameters for TAMie are included in parentheses.

	TraPPE (TraPPE-2)			Potoff (S/L)		
United-atom	ϵ (K)	σ (nm)	n	ϵ (K)	σ (nm)	n
CH_3	98 (134.5)	0.375 (0.352)	12	121.25	0.3783	16
CH_2	46	0.395	12	61	0.399	16
CH	10	0.468	12	15 (15/14)	0.46 (0.47/0.47)	16
C	0.5	0.640	12	1.2 (1.45/1.2)	0.61 (0.61/0.62)	16
	AUA4			TAMie		
CH_3	120.15	0.3607	12	136.318 (130.780)	0.36034 (0.36463)	14
CH_2	86.29	0.3461	12	52.9133	0.40400	14
CH	50.98	0.3363	12	14.5392	0.43656	14
C	15.04	0.244	12	–	–	–

Non-bonded interactions between two different site types (i.e. cross-interactions) are determined using Lorentz-Berthelot combining rules [3] for ϵ and σ, respectively, and an

arithmetic mean for the repulsive exponent n (as recommended in Reference 12):

$$\epsilon_{ij} = \sqrt{\epsilon_{ii}\epsilon_{jj}} \tag{4}$$

$$\sigma_{ij} = \frac{\sigma_{ii} + \sigma_{jj}}{2} \tag{5}$$

$$n_{ij} = \frac{n_{ii} + n_{jj}}{2} \tag{6}$$

where the ij subscript refers to cross-interactions and the subscripts ii and jj refer to same-site interactions.

2.2. Simulation set-up

Viscosity estimates can be obtained from both equilibrium molecular dynamics (EMD) and non-equilibrium molecular dynamics (NEMD) simulations. The "Best Practices Guide" is currently limited to EMD methods and purports that NEMD might be necessary for high viscosities (greater than 0.02 Pa-s). One purpose of the present work is to demonstrate that, by applying these guidelines, EMD can also provide meaningful estimates for highly viscous systems.

Equilibrium molecular dynamics simulations are performed using GROMACS version 2018 [18]. Example GROMACS input files (.top, .gro. and .mdp) are provided as Supporting Information. In addition, the shell and python scripts used for preparing and analyzing simulations are available on GitHub. The simulation specifications are provided in Tables 5 and 6.

Note that the non-bonded cut-off distance is 1.4 nm for each force field except Potoff, which employs a 1.0 nm cut-off (as recommended by the authors). Also, notice that the production time depends on the system, i.e., the compound and state point, where larger compounds, lower temperatures, and higher densities necessitate longer simulations. For most systems, 1 ns is a sufficient production time, while an 8 ns production time is required for the most viscous systems, e.g., 2,2,4-trimethylpentane at elevated pressures. Following "Best Practices", we compute η with several different production times (1, 2, 4, and 8 ns) for select systems to verify that the results are indistinguishable (see Supporting Information).

Table 5: General simulation specifications.

Time-step (fs)	2
Equilibration time (ns)	1
Production time (ns)	1, 2, 4, or 8
Cut-off length (nm)	1.4 (1.0 Potoff)
Tail-corrections [19]	U and P
Constraints	LINCS
LINCS-order	8
Number of molecules	400

Table 6: Integrator, thermostat and barostat specifications.

	NPT Equil.	NPT Prod.	NVT Equil.	NVT Prod.
Integrator	Velocity Verlet	Leap frog	Velocity Verlet	Velocity Verlet
Thermostat	Velocity rescale	Nosé-Hoover	Nosé-Hoover	Nosé-Hoover
Thermostat time-constant (ps)	1.0	1.0	1.0	1.0
Barostat	Berendsen	Parrinello-Rahman	N/A	N/A
Barostat time-constant (ps)	1.0	5.0	N/A	N/A
Barostat compressibility	4.5e-5	4.5e-5	N/A	N/A

Furthermore, we investigate system size effects by comparing results with 100, 200, 400, and 800 molecules (see Supporting Information). In addition, we compare fixed and flexible bonds in the Supporting Information.

As recommended by "Best Practices," we utilize 30 to 60 independent replicates to improve the precision and to provide more rigorous estimates of uncertainty. To ensure independence between replicates, a series of MD simulations are performed for each replicate. When the viscosity is desired at a prescribed temperature and density ($\eta(\rho, T)$), three stages

are required: energy minimization, NVT equilibration, and NVT production. When the viscosity is desired at a prescribed temperature and pressure ($\eta(P,T)$), five stages are required: energy minimization, NPT equilibration, NPT production, NVT equilibration, and NVT production. Note that, according to "Best Practices", the final production stage simulations are always performed using the NVT ensemble.

Two different classes of viscosity are investigated in this study, namely, saturated liquid viscosity ($\eta_{\text{liq}}^{\text{sat}}$) and compressed liquid viscosities at $T = 293$ K ($\eta_{\text{liq}}^{\text{comp}}$).

Saturated liquid viscosities are estimated by performing NVT ensemble simulations at various temperatures (T^{sat}) and densities ($\rho_{\text{liq}}^{\text{sat}}$). The simulation densities correspond to the REFPROP $\rho_{\text{liq}}^{\text{sat}}$, which is admittedly not equivalent to the force field $\rho_{\text{liq}}^{\text{sat}}$. This point is discussed in greater detail in Section 4.

Two different simulation protocols are implemented for estimating compressed liquid viscosities ($\eta_{\text{liq}}^{\text{comp}}$). Specifically, we perform simulations with each force field either at the same ρ or the same P. For the purpose of comparing trends between force fields and REFPROP, these two methods are essentially equivalent. From a practical standpoint, estimating η at a given P requires performing preliminary NPT ensemble simulations to determine the corresponding box size.

2.3. Data analysis

Following the "Best Practices" recommendation, we implement the Green-Kubo "time-decomposition" analysis to extract viscosity from EMD simulations. We refer the interested reader to References BLANK and BLANK for further details. In brief, the Green-Kubo integral is computed with respect to time according to

$$\frac{V}{3k_{\text{B}}TN_{\text{reps}}}\sum_{n=1}^{N_{\text{reps}}}\sum_{\alpha\neq\beta}\int_0^\infty dt\,\langle\tau_{\alpha\beta,n}(t)\tau_{\alpha\beta,n}(0)\rangle_{t_0} \tag{7}$$

where V is the volume, k_{B} is the Boltzmann constant, $\langle\cdots\rangle_{t_0}$ denotes an average over time origins, α and $\beta = x, y$, or z Cartesian coordinates, and $\tau_{\alpha\beta,n}$ is the α-β off-diagonal stress tensor element for the n^{th} replicate.

$\tau_{\alpha\beta,n}$ is recorded every 6 fs (3 time-steps) to adequately integrate the initial rapid decay of the autocorrelation function. To improve precision, Equation 7 is an average over all three off-diagonal components of the stress tensor, 30 to 60 independent replicate simulations (N_{reps}), and twelve different time-origins (t_0) for each replicate.

Since Equation 7 requires $t \to \infty$ and the "running integral" can become quite noisy at long times, it is important to fit the "running integral" to a function that can be extrapolated to the "true" infinite time limit (η^{∞}). Per "Best Practices", we use a double-exponential function for this purpose

$$\eta(t) = A\alpha\tau_1 \left(1 - \exp\left(-t/\tau_1\right)\right) + A(1-\alpha)\tau_2 \left(1 - \exp\left(-t/\tau_2\right)\right) \tag{8}$$

where A, α, τ_1, and τ_2 are fitting parameters and $\eta^{\infty} = A\alpha\tau_1 + A(1-\alpha)\tau_2$.

To account for the increasing fluctuations in the "running integral" with respect to time, Equation 8 is fit by minimizing a weighted sum-squared error objective function. The weight model, At^{-b}, is fit to the standard deviation (σ_η) of the replicate simulations. In addition, following a heuristic proposed by Zhang et al., data are excluded where $\sigma_\eta > 40$ % η^{∞}. As large fluctuations also exist at very short times, only data for $t > 3$ ps are included in the parameterization of Equation 8.

Uncertainties are obtained by bootstrap re-sampling. Specifically, the process described previously is repeated hundreds of times using randomly selected sets of replicate simulations. Furthermore, each repetition uses a randomly selected long-time cut-off between 30 % η^{∞} and 50 % η^{∞}. A 95 % confidence interval is obtained from the distribution of bootstrap estimates for η_{∞}. An example of this process is provided as Supporting Information.

3. Results

Six normal and seven branched alkanes of varying chain-length and degree of branching are simulated in this study. We only consider compounds with available REFPROP equations-of-state and viscosity correlations [20]. Specifically, we simulate ethane [21, 22], propane [23], *n*-butane [24, 25], *n*-octane [26, 27], *n*-dodecane [28, 29], *n*-hexadecane [30, 31], 2-methylpropane [32, 33], 2-methylbutane [32, 34], 2-methylpentane [32, 34], 3-methylpentane

[35, 34], 2,2-dimethylpropane [32, 34], 2,3-dimethylbutane [35, 34], and 2,2,4-trimethylpentane [36, 34].

Each compound was simulated using the TraPPE (UA LJ 12-6) and Potoff S/L (UA Mie 16-6) force fields. Potoff "short" parameters are used for 2-methylpropane, 2-methylbutane, 2,2-dimethylpropane, and 2,3-dimethylbutane while Potoff "long" parameters are utilized for 2-methylpentane, 3-methylpentane, and 2,2,4-trimethylpentane. Only 2,2-dimethylpropane was simulated with AUA4 (AUA LJ 12-6) while 2,2-dimethylpropane and 2,2,4-trimethylpentane were not simulated using the TAMie (AUA Mie 14-6) force field.

Table 7 demonstrates which compounds, force fields, and viscosity types were simulated in this study.

3.1. Saturated Liquid

3.1.1. n-Alkanes

Figure 1 compares the TraPPE (UA LJ 12-6), TraPPE-2 (AUA LJ 12-6), TAMie (AUA Mie 14-6), Potoff (UA Mie 16-6), and the Bayesian parameter sets for n = 13, 14, 15, and 16.

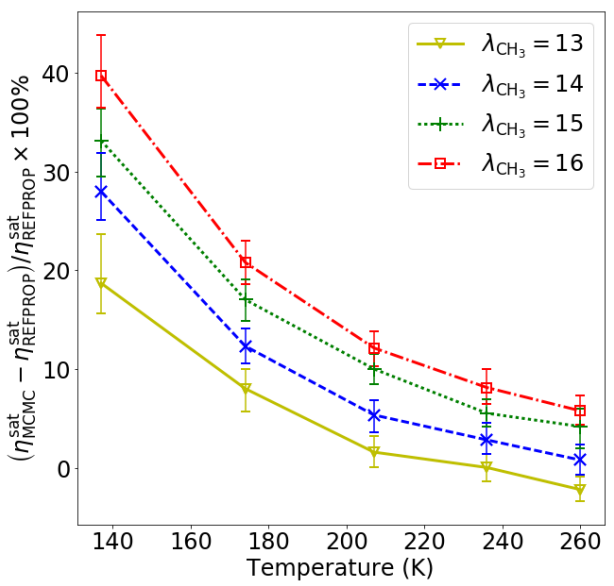

Figure 1: Saturated liquid viscosities for ethane. Colors/symbols denote different force fields.

Table 7: Compounds, force fields, and state points. "X": simulated, "O": not simulated, "S" simulated with "Short" parameters, "L" simulated with "Long" parameters.

	TraPPE (TraPPE-2)		Potoff (S/L)		AUA4		TAMie	
Compound	$\eta_{\text{liq}}^{\text{sat}}$	$\eta_{\text{liq}}^{\text{comp}}$	$\eta_{\text{liq}}^{\text{sat}}$	$\eta_{\text{liq}}^{\text{comp}}$	$\eta_{\text{liq}}^{\text{sat}}$	$\eta_{\text{liq}}^{\text{comp}}$	$\eta_{\text{liq}}^{\text{sat}}$	$\eta_{\text{liq}}^{\text{comp}}$
ethane	X	X	X	X	X	X	X	X
propane	X	X	X	X	O	O	X	X
n-butane	X	X	X	X	O	O	X	X
n-octane	X	X	X	X	O	O	X	X
n-dodecane	X	O	X	O	O	O	X	O
n-hexadecane	X	O	X	O	O	O	X	O
2-methylpropane	X	X	S	S	O	O	X	X
2-methylbutane	X	X	S	S	O	O	X	X
2,2-dimethylpropane	X	X	S	S	X	X	O	O
2,3-dimethylbutane	X	X	S	S	O	O	X	X
2-methylpentane	X	X	L	L	O	O	X	X
3-methylpentane	X	X	L	L	O	O	X	X
2,2,4-trimethylpentane	X	X	L	L	O	O	O	O

Figure 2 compares the TraPPE (UA LJ 12-6), Potoff (UA Mie 16-6), and TAMie (AUA Mie 14-6) saturated liquid viscosities for propane, n-butane, and n-octane. Similar to what has been demonstrated in previous studies, the TraPPE force field significantly under predicts $\eta_{\text{liq}}^{\text{sat}}$ (between 30 and 80 %) with the deviation increasing towards the triple point temperature. By contrast, the Potoff and TAMie force fields agree with the REFPROP values for these compounds to within 10 % over the entire temperature range studied (which includes the triple point for propane), and do not demonstrate a strong temperature dependence.

Figure 3 compares the TraPPE, Potoff, and TAMie saturated liquid viscosities for n-dodecane and n-hexadecane. Although the TAMie and TraPPE results for these compounds

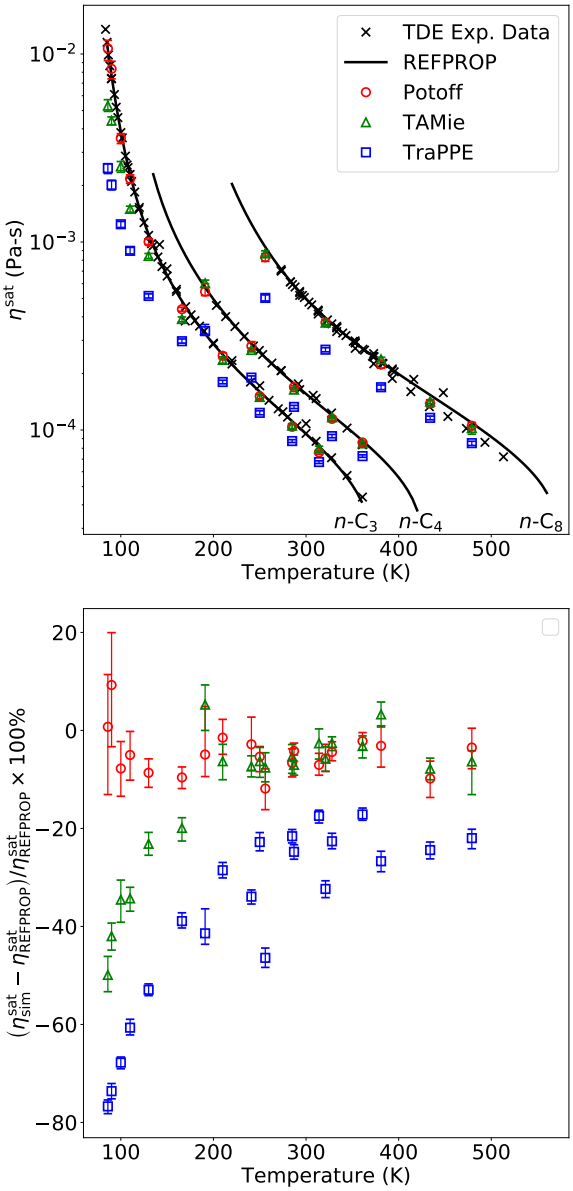

Figure 2: Saturated liquid viscosities for propane, n-butane, and n-octane. Colors/symbols denote different force fields.

are similar to those observed in Figure 2, it is quite curious that the Potoff results are nearly identical to the TraPPE results for n-dodecane (which significantly under predict η^{sat}).

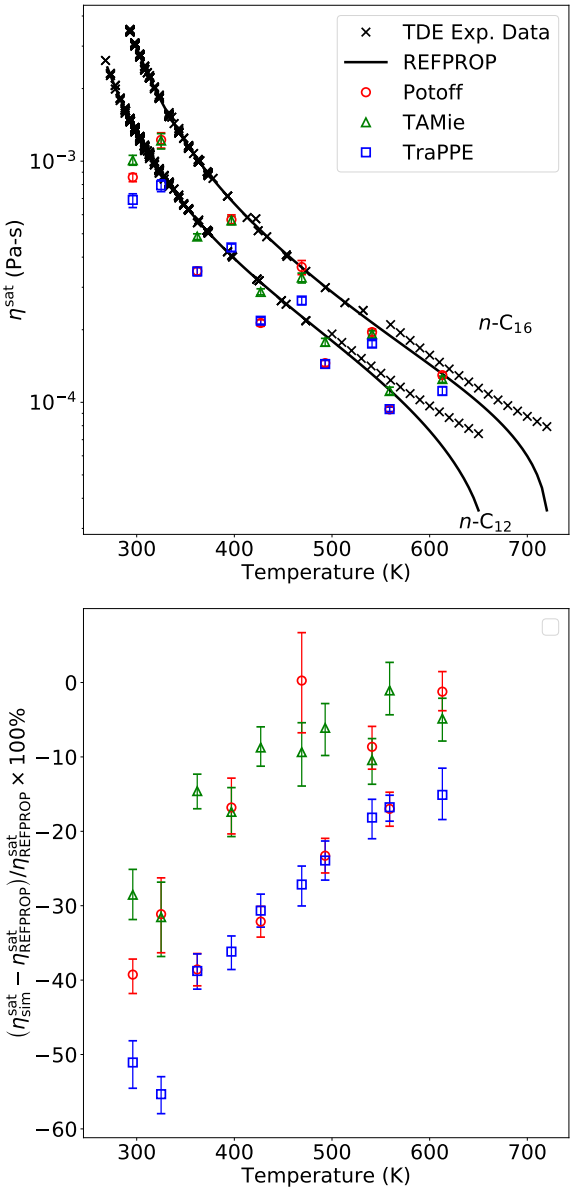

Figure 3: Saturated liquid viscosities for n-dodecane and n-hexadecane. Colors/symbols denote different force fields.

3.1.2. Branched alkanes

Figures 4 and 5 compare the saturated liquid viscosities for each force field and branched alkane studied. Figures 4 and 5 present results for the compounds classified by Potoff as "short" and "long", respectively. Specifically, Figure 4 depicts 2-methylpropane, 2,2-

dimethylpropane, 2-methylbutane, and 2,3-dimethylbutane, while Figure 5 contains 2-methylpentane, 3-methylpentane, and 2,2,4-trimethylpentane. Each compound was simulated using the TraPPE (UA LJ 12-6) and Potoff (UA Mie 16-6) force fields. However, only 2,2-dimethylpropane was simulated with AUA4 (AUA LJ 12-6) while 2,2-dimethylpropane and 2,2,4-trimethylpentane were not simulated using the TAMie (AUA Mie 14-6) force field.

From Figures 4 and 5, we see that the Potoff S/L and TAMie force fields are not as accurate for these branched alkanes as for the normal alkanes. In particular, Potoff and TAMie demonstrates the same temperature dependence observed for other force fields, where the deviations are largest at lower temperatures. However, Potoff still provides considerable improvement compared to the LJ 12-6 based models, i.e., TraPPE and AUA4. Note that the performance is similar for the Potoff "short" and "long" parameters in Figures 4 and 5, respectively.

The deviations for each force field are largest for 2-methylpropane and 2,2-dimethylpropane. Since these compounds are primarily composed of CH_3 UA sites, this poor performance is likely due to the assumption that the CH_3 non-bonded parameters are transferable from n-alkanes to branched alkanes. Improvement might be possible if the CH_3 parameters were different depending on the neighboring UA site type.

3.2. Compressed liquid

Section 3.1 demonstrated that Mie n-6 based force fields (Potoff and TAMie) are considerably more reliable for predicting saturated liquid viscosities than LJ 12-6 based force fields (TraPPE and AUA4). However, both the Potoff and TAMie non-bonded potentials use $n > 12$. Reference BLANK demonstrates that $n > 12$ leads to strong negative consequences at high densities/pressures. Specifically, $n > 12$ is too repulsive at short distances which leads to over estimates of pressure at high densities. For this reason, this section compares the different force fields above saturation pressure.

3.2.1. n-Alkanes

Figures 6, 7, and 8 compare the elevated pressure viscosities for propane, n-butane, and n-octane, respectively. Each compound is simulated using the TraPPE, Potoff, and TAMie

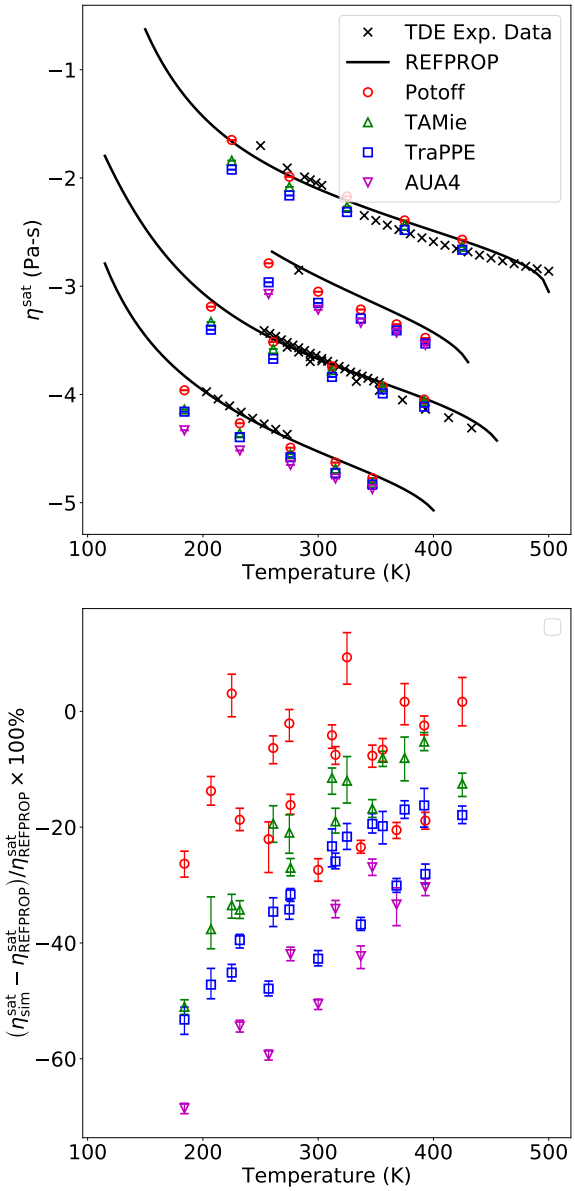

Figure 4: Saturated liquid viscosities for 2-methylpropane, 2,2-dimethylpropane, 2-methylbutane, and 2,3-dimethylbutane. Colors/symbols denote different force fields.

force fields. Note that for propane and n-butane (Figures 6 and 7) each force field is simulated at the same density, while for n-octane (Figure 8) the force fields are simulated at the same pressure.

Figure 6 demonstrates that the TraPPE force field has a constant negative bias even with

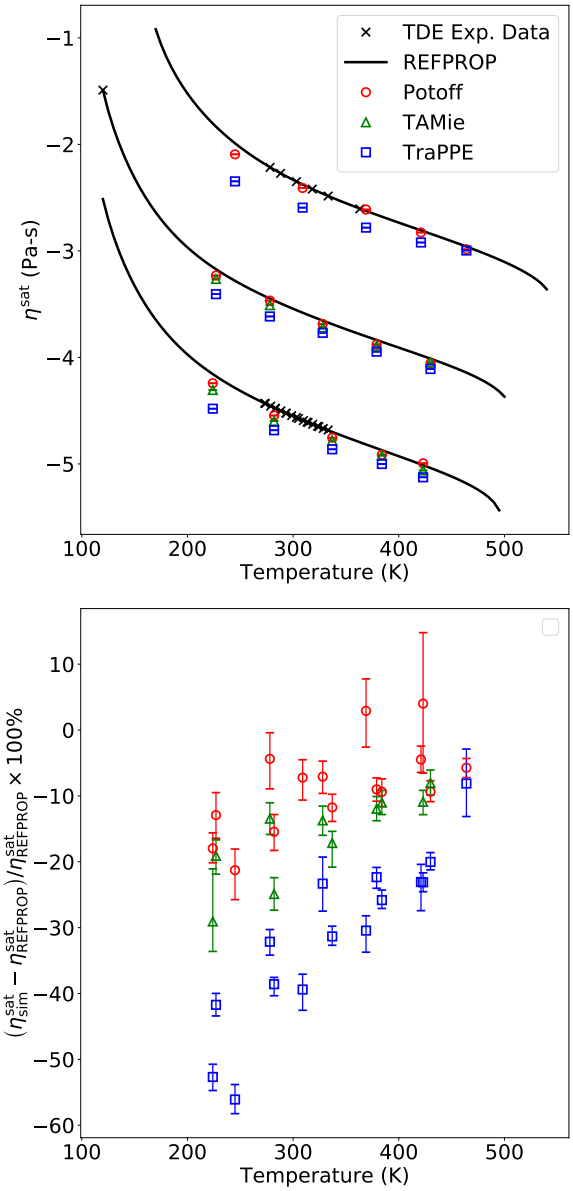

Figure 5: Saturated liquid viscosities for 2-methylpentane, 3-methylpentane, and 2,2,4-trimethylpentane. Colors/symbols denote different force fields.

increasing density/pressure. The TAMie force field has the most accurate η-ρ dependence, i.e., the error does not increase with respect to density. By contrast, the Potoff potential demonstrates considerable over estimation of η at high densities, which is likely attributed to the overly repulsive Mie 16-6 potential at close distances. Remarkably, the Potoff force

field is the most accurate at predicting the η-P dependence. This can be explained as a cancellation of errors since the Potoff force field significantly over predicts both viscosity and pressure at high densities.

The results in Figures 7 and 8 for n-butane and n-octane, respectively, are similar to those in Figure 6 for propane. Specifically, the TraPPE force field under predicts η at all densities/pressures, the TAMie force field provides the most accurate η-ρ dependence, while the Potoff force field over predicts η-ρ dependence but accurately predicts the η-P dependence.

3.2.2. Branched alkanes

The trends observed in Figures 9 to 12 are consistent with the compressed liquid trends for n-alkanes. Specifically, TraPPE under-predicts the viscosity with respect to both ρ and P. Potoff over-predicts η with respect to ρ but provides a reasonable estimate for η with respect to P. However, as observed previously for saturation viscosities, Potoff and TAMie are less accurate for branched alkanes than for n-alkanes.

4. Discussion/Limitations

1. Discussion
   (a) Mie potentials parameterized with VLE data provide significant improvement over LJ 12-6
   (b) Potoff over-predicts $\eta - \rho$ dependence while TAMie is fairly accurate
   (c) Potoff appears to be slightly more accurate for $\eta - P$
   (d) Branched alkanes are not as accurate, perhaps assumption of transferability or torsional parameters
2. Limitations
   (a) Largest viscosity simulations are slow to converge and unclear if simulations are sufficiently long
   (b) Tail-corrections could impact dynamics
   (c) Using REFPROP saturation conditions instead of force fields

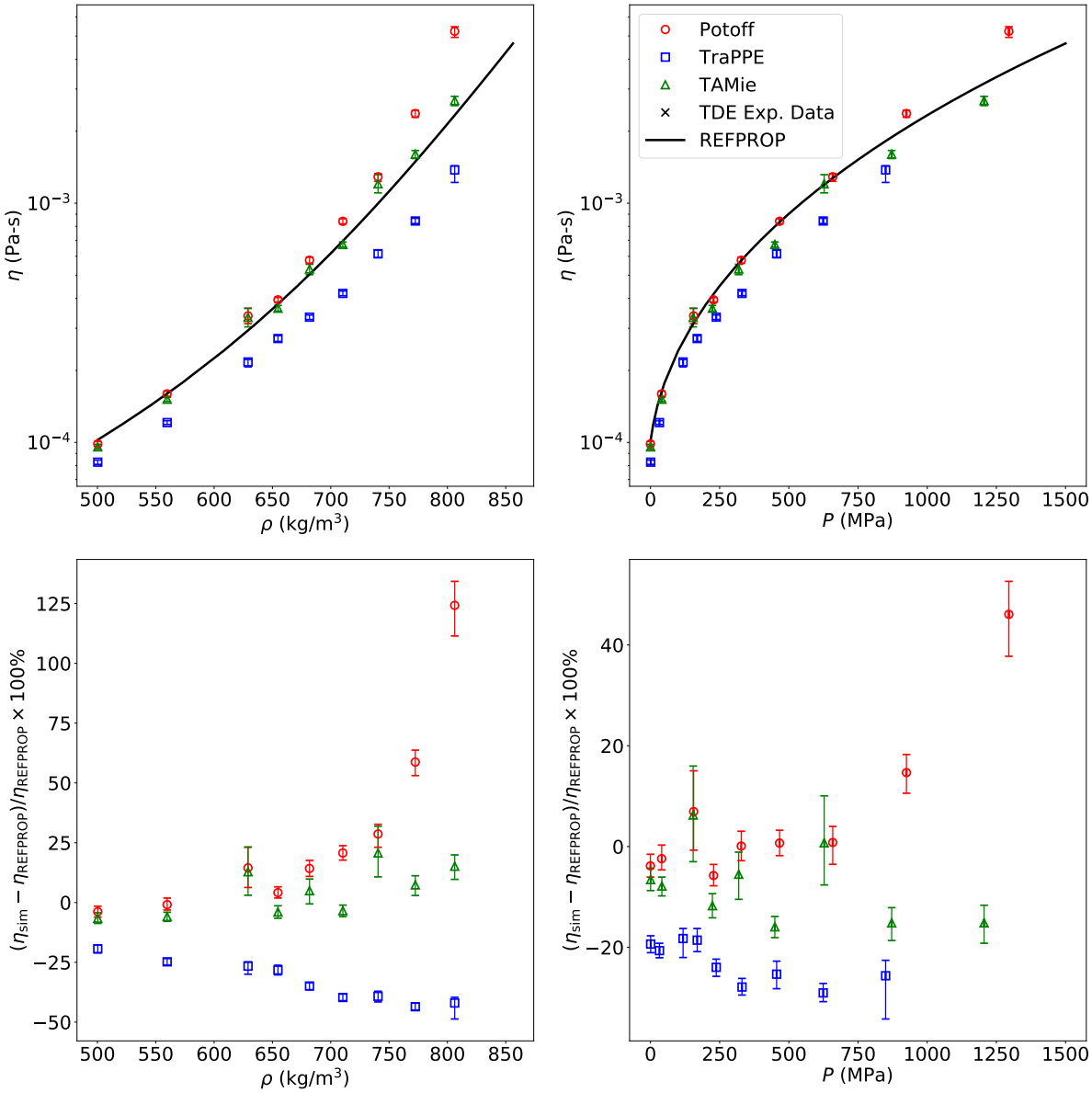

Figure 6: Compressed liquid viscosities at 293 K for propane. Colors/symbols denote different force fields.

4.1. $\rho_{\text{liq}}^{\text{sat}}$

There are at least three reasons why we perform simulations at the REFPROP $\rho_{\text{liq}}^{\text{sat}}$ instead of the force field $\rho_{\text{liq}}^{\text{sat}}$. First, this approach allows for a fair comparison of the force fields' ability to predict viscosity, without penalizing force fields which are less accurate at predicting $\rho_{\text{liq}}^{\text{sat}}$ or rewarding force fields that mask their deficiencies in predicting viscosity by

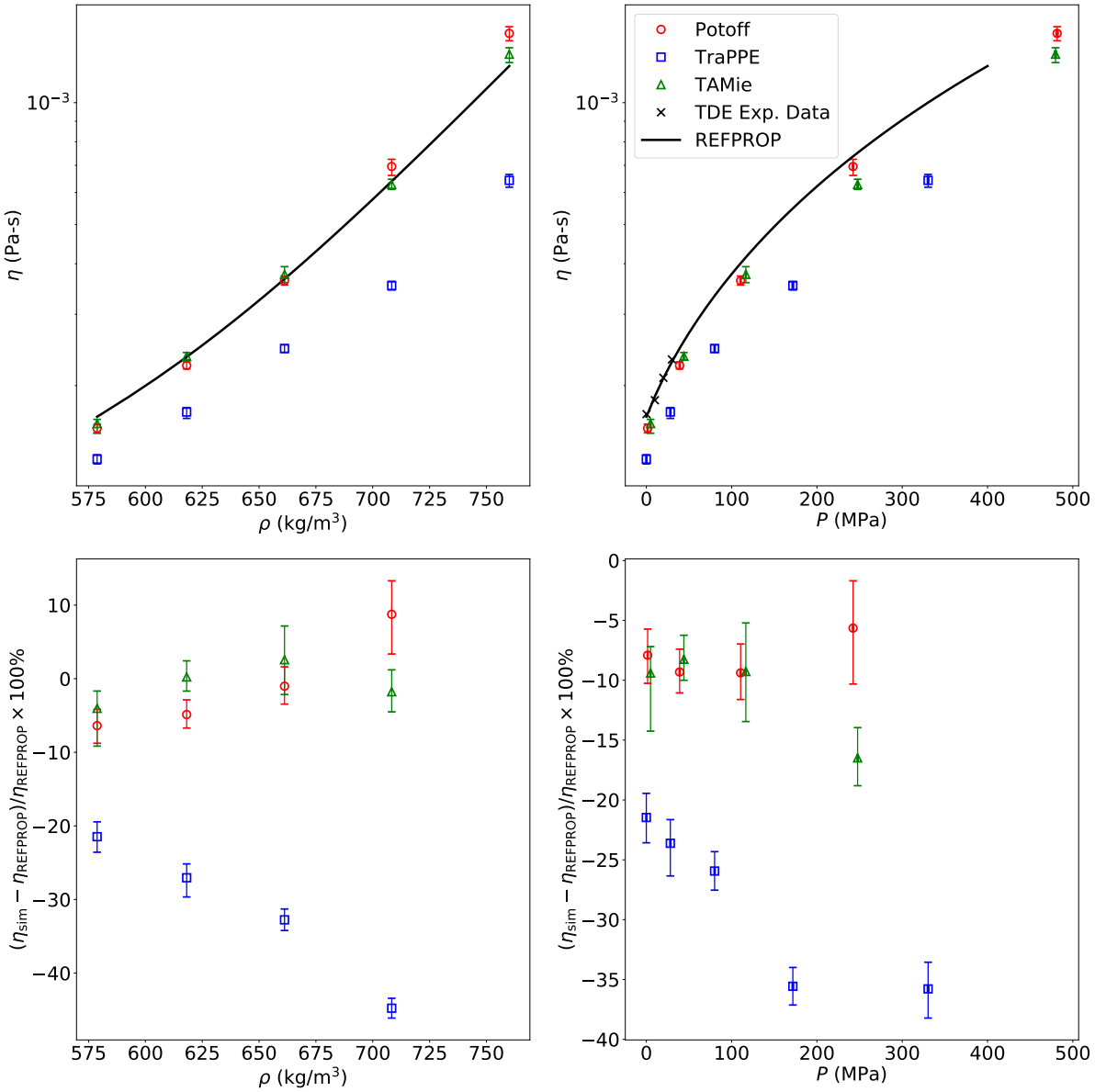

Figure 7: Compressed liquid viscosities at 293 K for n-butane. Colors/symbols denote different force fields.

over- or under-estimating ρ_{liq}^{sat}. Second, since each of the studied force fields utilized ρ_{liq}^{sat} data in their optimization, deviations between the REFPROP and force field values are small, typically less than 1 %. However, small differences in density have been reported to result in large differences in viscosity. For this reason, a small set of validation simulations are performed to determine the variability caused by utilizing the REFPROP densities. The

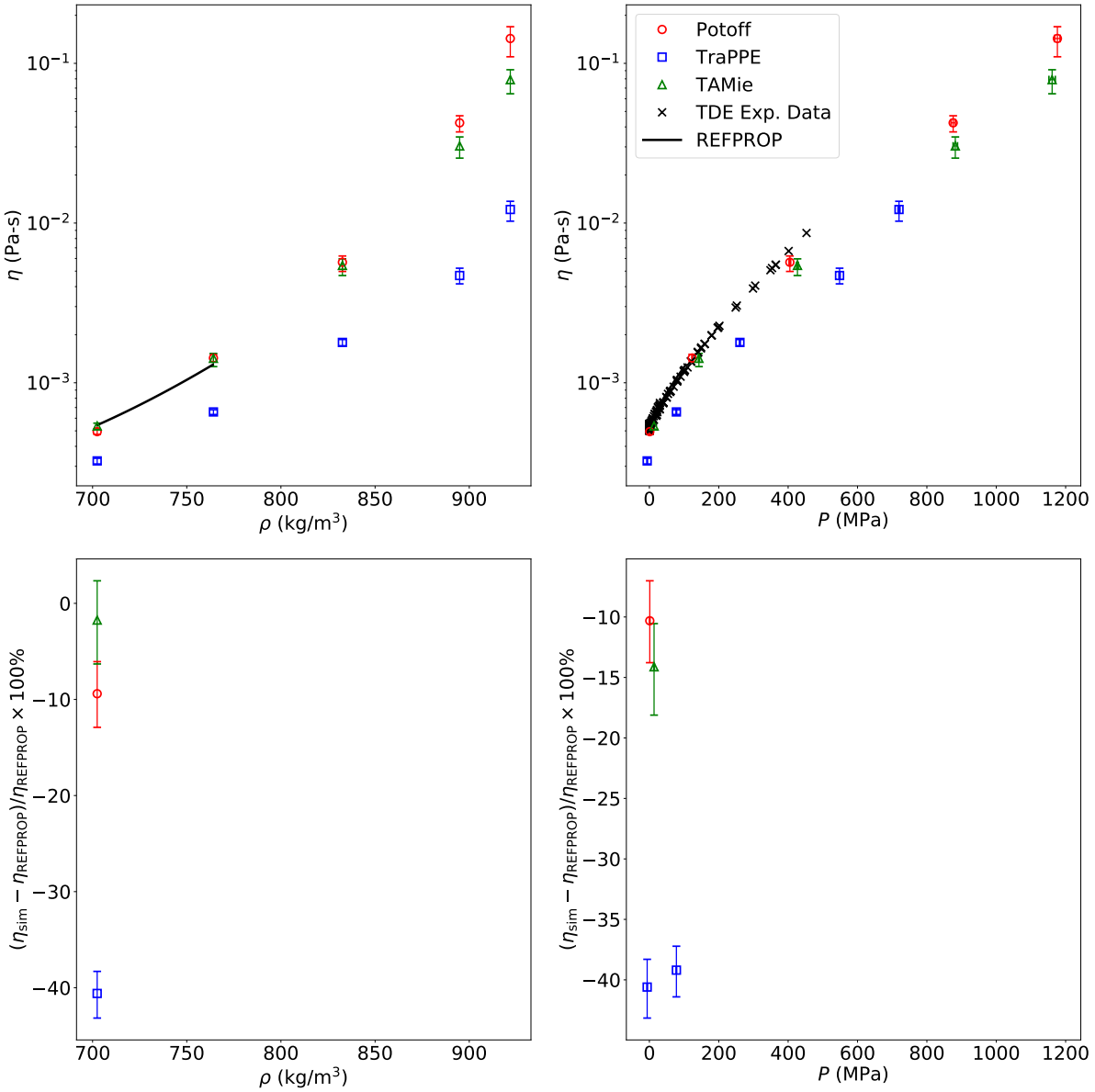

Figure 8: Compressed liquid viscosities at 293 K for n-octane. Colors/symbols denote different force fields.

force field saturated liquid densities were obtained from the literature.

The use of REFPROP $\rho_{\text{liq}}^{\text{sat}}$ caused some simulations to be in a meta-stable state. Specifically, this occurs when the force field vapor pressure is less than the REFPROP vapor pressure. Fortunately, this is uncommon as Potoff, TAMie, and AUA4 are quite reliable for estimating $P_{\text{vap}}^{\text{sat}}$ and TraPPE significantly over-estimates $P_{\text{vap}}^{\text{sat}}$.

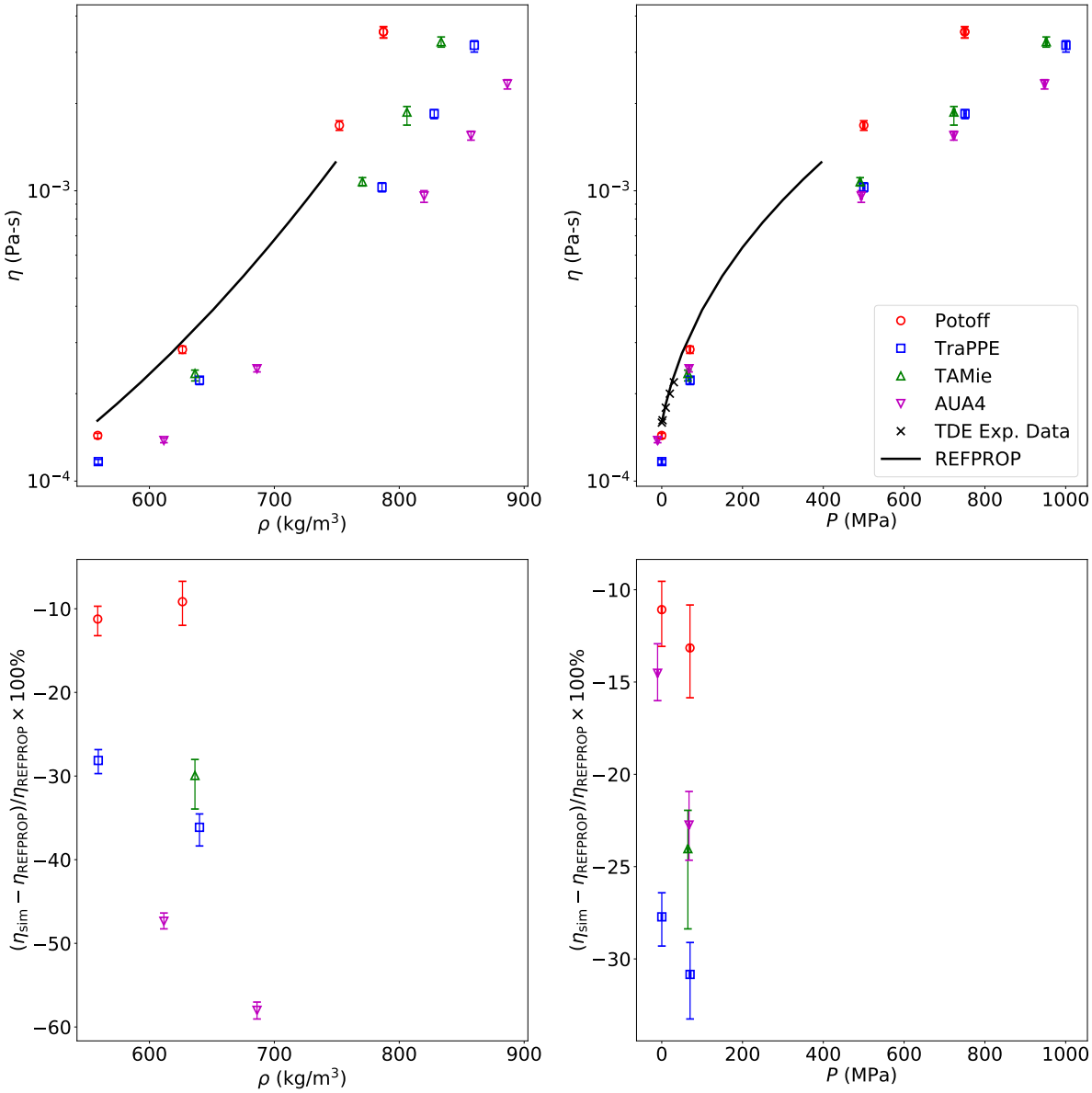

Figure 9: Compressed liquid viscosities at 293 K for 2-methylpropane. Colors/symbols denote different force fields.

5. Conclusions

This study demonstrates the improvement that has taken place over the past two decades for predicting viscosity with molecular simulation. First, the "Best Practices" for EMD lead to more reproducible results. Second, the state-of-the-art Mie n-6 force fields are significantly

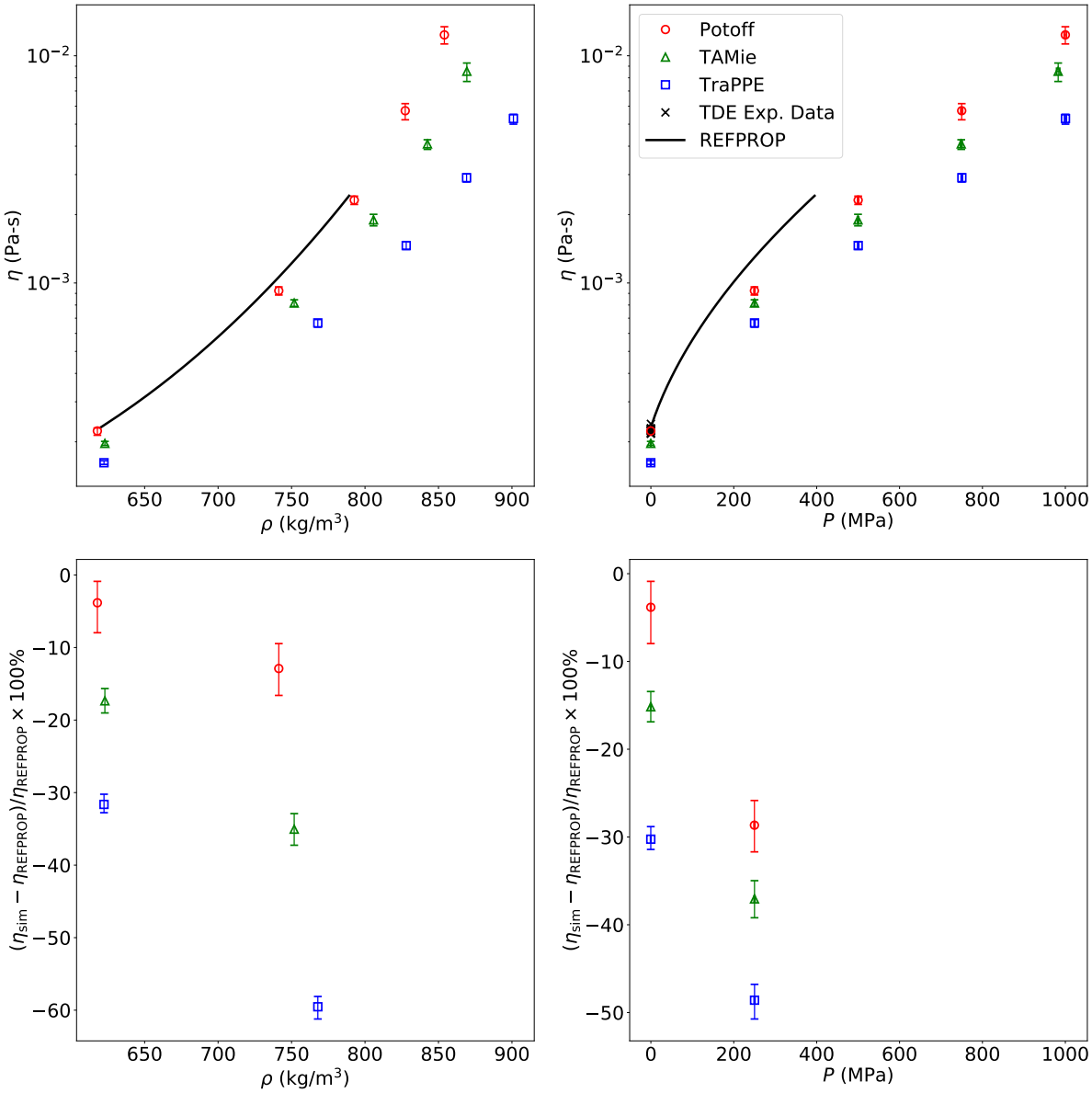

Figure 10: Compressed liquid viscosities at 293 K for 2-methylbutane. Colors/symbols denote different force fields.

more accurate than the traditional Lennard-Jones 12-6 force fields. More specifically, the Potoff and TAMie force fields typically predict saturated liquid viscosities for n-alkanes to within 10 % of the REFPROP values. By contrast, the TraPPE and AUA4 models under-predict saturated liquid viscosities by 30 % to 50 %, where the deviations are largest at

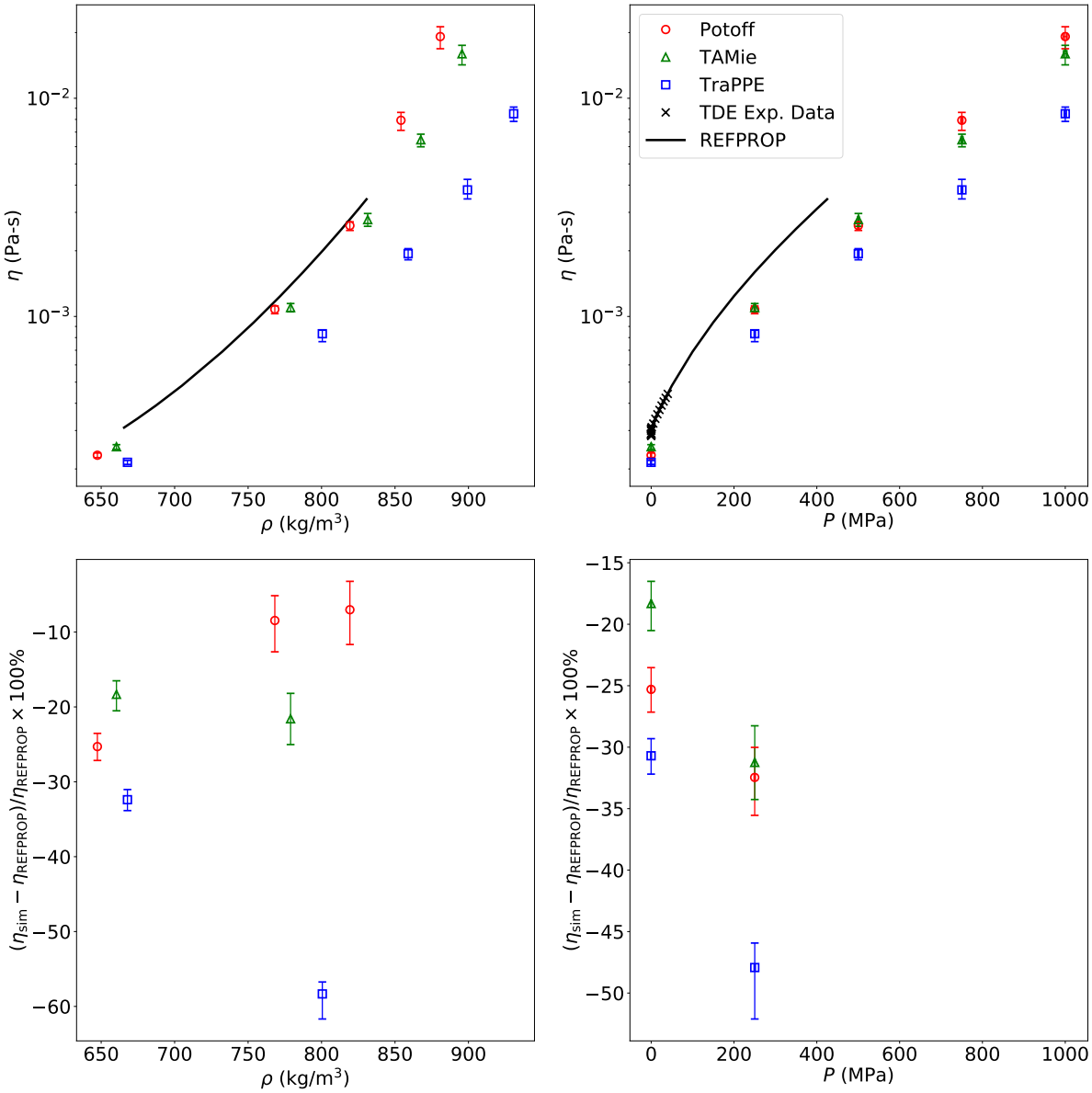

Figure 11: Compressed liquid viscosities at 293 K for 3-methylpentane. Colors/symbols denote different force fields.

lower temperatures. While Potoff and TAMie are also more reliable for branched alkanes, deviations are larger and demonstrate a similar temperature dependence. The key limitation of the Potoff force field is that the choice of n= 16 is too repulsive at high densities, which causes the viscosity to be over-estimated at high densities. Due to a fortuitous cancellation

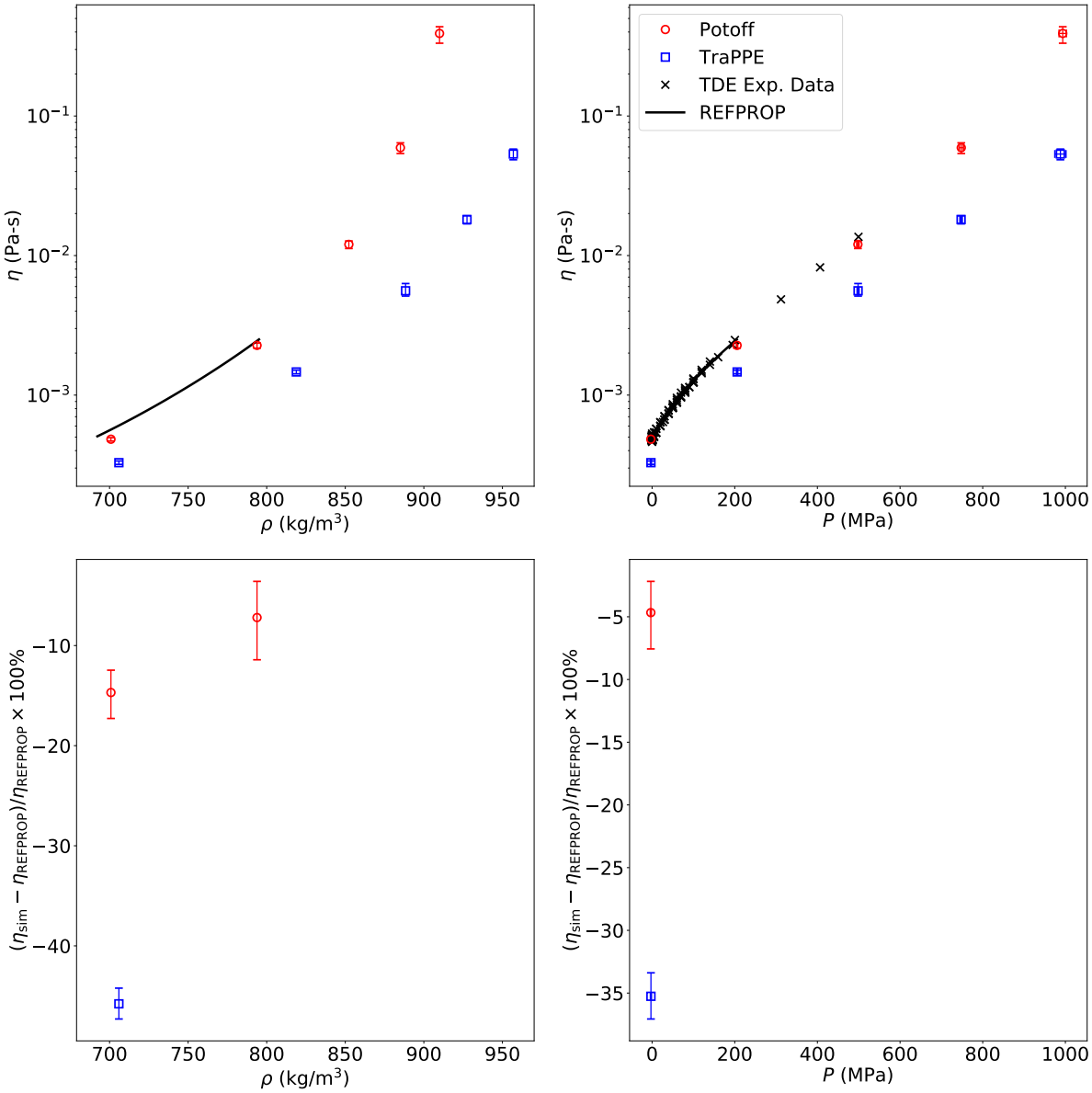

Figure 12: Compressed liquid viscosities at 293 K for 2,2,4-trimethylpentane. Colors/symbols denote different force fields.

of errors, the Potoff potential does provide a reliable η-P trend. Since TAMie uses n= 14, the η-ρ trend is slightly more reliable than that of Potoff.

Acknowledgments

We are grateful for the internal review provided by NIST BERB Reviewer 1 and NIST BERB Reviewer 2 from the National Institute of Standards and Technology (NIST).

This research was performed while Richard A. Messerly held a National Research Council (NRC) Postdoctoral Research Associateship at NIST and while Michelle C. Anderson held a Summer Undergraduate Research Fellowship (SURF) position at NIST.

References

[1] Edward J. Maginn, Richard A. Messerly, Daniel J. Carlson, Daniel R. Roe, and J. Richard Elliott. Best practices for computing transport properties 1. self-diffusivity and viscosity from equilibrium molecular dynamics v1. *Molecular Simulation*, Pending publication, 2018.

[2] Peter A. Gordon. Development of intermolecular potentials for predicting transport properties of hydrocarbons. *The Journal of Chemical Physics*, 125(1):014504, 2006.

[3] M. P. Allen and D. J. Tildesley. *Computer Simulation of Liquids*. Clarendon Press ; Oxford University Press, Oxford England New York, 1987.

[4] Rajdeep Singh Payal, S. Balasubramanian, Indranil Rudra, Kunj Tandon, Ingo Mahlke, David Doyle, and Roger Cracknell. Shear viscosity of linear alkanes through molecular simulations: quantitative tests for n-decane and n-hexadecane. *Molecular Simulation*, 38(14-15):1234–1241, 2012.

[5] Maurizio Mondello and Gary S. Grest. Viscosity calculations of n-alkanes by equilibrium molecular dynamics. *The Journal of Chemical Physics*, 106(22):9327–9336, 1997.

[6] Molecular simulation of the thermophysical properties of fluids: From understanding toward quantitative predictions. *Journal of Molecular Liquids*, 134(1):71 – 89, 2007. EMLG/JMLG 2005 Special Issue.

[7] Hai Hoang, StÃľphanie Delage-Santacreu, and Guillaume Galliero. Simultaneous description of equilibrium, interfacial, and transport properties of fluids using a mie chain coarse-grained force field. *Industrial & Engineering Chemistry Research*, 56(32):9213–9226, 2017.

[8] Carmelo Herdes, Tim S. Totton, and Erich A. Müller. Coarse grained force field for the molecular simulation of natural gases and condensates. *Fluid Phase Equilibria*, 406:91 – 100, 2015.

[9] M. G. Martin and J. I. Siepmann. Transferable potentials for phase equilibria. 1. United-atom description of n-alkanes. *The Journal of Physical Chemistry B*, 102(14):2569–2577, 1998.

[10] Marcus G. Martin and J. Ilja Siepmann. Novel configurational-bias monte carlo method for branched molecules. Transferable Potentials for Phase Equilibria. 2. United-Atom Description of Branched Alkanes. *The Journal of Physical Chemistry B*, 103(21):4508–4517, 1999.

[11] Mansi S. Shah, J. Ilja Siepmann, and Michael Tsapatsis. Transferable potentials for phase equilibria. Improved united-atom description of ethane and ethylene. *AIChE Journal*, 63(11):5098–5110, 2017.

[12] J. J. Potoff and D. A. Bernard-Brunel. Mie potentials for phase equilibria calculations: Applications to alkanes and perfluoroalkanes. *The Journal of Physical Chemistry B*, 113(44):14725–14731, 2009.

[13] Jason R. Mick, Mohammad Soroush Barhaghi, Brock Jackman, Loren Schwiebert, and Jeffrey J. Potoff. Optimized mie potentials for phase equilibria: Application to branched alkanes. *Journal of Chemical & Engineering Data*, 62(6):1806–1818, 2017.

[14] Philippe Ungerer, Christele Beauvais, Jerome Delhommelle, Anne Boutin, Bernard Rousseau, and Alain H. Fuchs. Optimization of the anisotropic united atoms inter-

molecular potential for n-alkanes. *The Journal of Chemical Physics*, 112(12):5499–5510, 2000.

[15] Carlos Nieto-Draghi, Anthony Bocahut, Benoît Creton, Pascal Have, Aziz Ghoufi, Aurélie Wender, , Anne Boutin, Bernard Rousseau, and Laurent Normand. Optimisation of the dynamical behaviour of the anisotropic united atom model of branched alkanes: application to the molecular simulation of fuel gasoline. *Molecular Simulation*, 34(2):211–230, 2008.

[16] Andrea Hemmen and Joachim Gross. Transferable anisotropic united-atom force field based on the Mie potential for phase equilibrium calculations: n-alkanes and n-olefins. *The Journal of Physical Chemistry B*, 119(35):11695–11707, 2015.

[17] Dominik Weidler and Joachim Gross. Transferable anisotropic united-atom force field based on the mie potential for phase equilibria: Aldehydes, ketones, and small cyclic alkanes. *Industrial & Engineering Chemistry Research*, 55(46):12123–12132, 2016.

[18] M.J. Abraham, D. van der Spoel, E. Lindahl, B.Hess, and the GROMACS development team. *GROMACS User Manual version 2018, www.gromacs.org (2018)*, 2018.

[19] GROMACS non-bonded tail corrections assume that the long-range contribution from the $r^{-\lambda}$ term is negligible compared to the r^{-6} term. By comparing the GROMACS output with other (slower) simulation packages, we verified that the small error introduced with this approximation does not significantly affect our results. For this reason, although it is straightforward to include the $r^{-\lambda}$ contribution, we did not attempt to modify the GROMACS default tail correction values.

[20] E. W. Lemmon, M. L. Huber, and M. O. McLinden. NIST Standard Reference Database 23: Reference Fluid Thermodynamic and Transport Properties-REFPROP, Version 9.1, National Institute of Standards and Technology, 2013.

[21] D. Bücker and W. Wagner. A reference equation of state for the thermodynamic prop-

erties of ethane for temperatures from the melting line to 675 K and pressures up to 900 MPa. *Journal of Physical and Chemical Reference Data*, 35(1):205–266, 2006.

[22] Eckhard Vogel, Roland Span, and Sebastian Herrmann. Reference correlation for the viscosity of ethane. *Journal of Physical and Chemical Reference Data*, 44(4):043101, 2015.

[23] Eric W. Lemmon, Mark O. McLinden, and Wolfgang Wagner. Thermodynamic properties of propane. iii. a reference equation of state for temperatures from the melting line to 650 K and pressures up to 1000 MPa. *Journal of Chemical & Engineering Data*, 54(12):3141–3180, 2009.

[24] D. Bücker and W. Wagner. Reference equations of state for the thermodynamic properties of fluid phase n-butane and isobutane. *Journal of Physical and Chemical Reference Data*, 35(2):929–1019, 2006.

[25] Sebastian Herrmann and Eckhard Vogel. New formulation for the viscosity of n-butane. *Journal of Physical and Chemical Reference Data*, 47(1):013104, 2018.

[26] R. Beckmueller, M. Thol, and R. Span. Fundamental equation of state for n-octane. *International Journal of Thermophysics*, Pending publication, 2018.

[27] Marcia L. Huber, Arno Laesecke, and Hong Wei Xiang. Viscosity correlations for minor constituent fluids in natural gas: n-octane, n-nonane and n-decane. *Fluid Phase Equilibria*, 224(2):263 – 270, 2004.

[28] Eric W. Lemmon and Marcia L. Huber. Thermodynamic properties of n-dodecane. *Energy & Fuels*, 18(4):960–967, 2004.

[29] Marcia L. Huber, Arno Laesecke, and Richard Perkins. Transport properties of n-dodecane. *Energy & Fuels*, 18(4):968–975, 2004.

[30] R. Romeo and E.W. Lemmon. To be submitted. 2018.

[31] Private communication to M. Huber from V. Vesovic, Oct. 2017.

[32] Eric W. Lemmon and Roland Span. Short fundamental equations of state for 20 industrial fluids. *Journal of Chemical & Engineering Data*, 51(3):785–850, 2006.

[33] E. Vogel, C. Küchenmeister, and E. Bich. Viscosity correlation for isobutane over wide ranges of the fluid region1. *International Journal of Thermophysics*, 21(2):343–356, Mar 2000.

[34] M.L. Huber. Models for the viscosity, thermal conductivity, and surface tension of selected pure fluids as implemented in refprop v10.0. *NISTIR 8209*, Pending publication, 2018.

[35] K. Gao, J. Wu, and E.W. Lemmon. Unpublished equation. 2017.

[36] T.M. Blackham, A.K. Lemmon, and E.W. Lemmon. Fundamental equation of state for isooctane. *International Journal of Thermophysics*, Pending publication, 2018.

6. Supporting Information

6.1. Gromacs input files

1. Include all the .gro files
2. Include all the .top file templates
3. Include .mdp files
4. Or we can just include an example and then refer them to the GitHub website

6.2. Tabulated values

1. Ethane
   (a) Saturation
      i. Potoff
      ii. TraPPE
      iii. AUA4

iv. TAMie

(b) T293 highP

i. Potoff

ii. TraPPE

iii. AUA4

iv. TAMie

2. Propane

(a) Saturation

i. Potoff

ii. TraPPE

iii. AUA4

iv. TAMie

(b) T293 highP

i. Potoff

ii. TraPPE

iii. AUA4

iv. TAMie

3. n-Butane

(a) Saturation

i. Potoff

ii. TraPPE

iii. AUA4

iv. TAMie

(b) T293 highP

i. Potoff

ii. TraPPE

iii. AUA4

iv. TAMie

Repeat for all other compounds with corresponding potentials

6.3. Finite-size effects

1. Simulation results for 100, 200, 400, and 800 molecules

6.4. Simulation length effects

1. Verified that 1 ns is long enough for larger compounds

6.5. Validation Runs

1. Ethane NIST
2. n-Octane Literature

6.6. Bond types, Harmonic vs LINCS

1. Propane and n-butane with harmonic (arbirary bond constant) shows systematic increase

6.7. Green-Kubo analysis

1. Raw data, i.e., multiple replicates with the average
2. Exclude low time data and have a heurestic for determining the cut-off time

Example analysis, i.e., bootstrap distribution, replicates

6.8. MCMC?